

Search for Darkonium in e^+e^- Collisions

J. P. Lees,¹ V. Poireau,¹ V. Tisserand,¹ E. Grauges,² A. Palano,³ G. Eigen,⁴ D. N. Brown,⁵ Yu. G. Kolomensky,⁵ M. Fritsch,⁶ H. Koch,⁶ T. Schroeder,⁶ R. Cheaib,^{b,7} C. Hearty^{ab,7} T. S. Mattison^{b,7} J. A. McKenna^{b,7} R. Y. So^{b,7} V. E. Blinov^{abc,8} A. R. Buzykaev^{a,8} V. P. Druzhinin^{ab,8} V. B. Golubev^{ab,8} E. A. Kozyrev^{ab,8} E. A. Kravchenko^{ab,8} A. P. Onuchin^{abc,8,*} S. I. Serednyakov^{ab,8} Yu. I. Skovpen^{ab,8} E. P. Solodov^{ab,8} K. Yu. Todyshev^{ab,8} A. J. Lankford,⁹ B. Dey,¹⁰ J. W. Gary,¹⁰ O. Long,¹⁰ A. M. Eisner,¹¹ W. S. Lockman,¹¹ W. Panduro Vazquez,¹¹ D. S. Chao,¹² C. H. Cheng,¹² B. Echenard,¹² K. T. Flood,¹² D. G. Hitlin,¹² J. Kim,¹² Y. Li,¹² D. X. Lin,¹² T. S. Miyashita,¹² P. Ongmongkolkul,¹² J. Oyang,¹² F. C. Porter,¹² M. Röhrken,¹² Z. Huard,¹³ B. T. Meadows,¹³ B. G. Pushpawela,¹³ M. D. Sokoloff,¹³ L. Sun,^{13,†} J. G. Smith,¹⁴ S. R. Wagner,¹⁴ D. Bernard,¹⁵ M. Verderi,¹⁵ D. Bettoni^{a,16} C. Bozzi^{a,16} R. Calabrese^{ab,16} G. Cibinetto^{ab,16} E. Fioravanti^{ab,16} I. Garzia^{ab,16} E. Luppi^{ab,16} V. Santoro^{a,16} A. Calcaterra,¹⁷ R. de Sangro,¹⁷ G. Finocchiaro,¹⁷ S. Martellotti,¹⁷ P. Patteri,¹⁷ I. M. Peruzzi,¹⁷ M. Piccolo,¹⁷ M. Rotondo,¹⁷ A. Zallo,¹⁷ S. Passaggio,¹⁸ C. Patrignani,^{18,‡} B. J. Shuve,¹⁹ H. M. Lacker,²⁰ B. Bhuyan,²¹ U. Mallik,²² C. Chen,²³ J. Cochran,²³ S. Prell,²³ A. V. Gritsan,²⁴ N. Arnaud,²⁵ M. Davier,²⁵ F. Le Diberder,²⁵ A. M. Lutz,²⁵ G. Wormser,²⁵ D. J. Lange,²⁶ D. M. Wright,²⁶ J. P. Coleman,²⁷ E. Gabathuler,^{27,*} D. E. Hutchcroft,²⁷ D. J. Payne,²⁷ C. Touramanis,²⁷ A. J. Bevan,²⁸ F. Di Lodovico,^{28,§} R. Sacco,²⁸ G. Cowan,²⁹ Sw. Banerjee,³⁰ D. N. Brown,³⁰ C. L. Davis,³⁰ A. G. Denig,³¹ W. Gradl,³¹ K. Griessinger,³¹ A. Hafner,³¹ K. R. Schubert,³¹ R. J. Barlow,^{32,¶} G. D. Lafferty,³² R. Cenci,³³ A. Jawahery,³³ D. A. Roberts,³³ R. Cowan,³⁴ S. H. Robertson^{ab,35} R. M. Seddon^{b,35} N. Neri^{a,36} F. Palombo^{ab,36} L. Cremaldi,³⁷ R. Godang,^{37,**} D. J. Summers,^{37,*} P. Taras,³⁸ G. De Nardo,³⁹ C. Sciacca,³⁹ G. Raven,⁴⁰ C. P. Jessop,⁴¹ J. M. LoSecco,⁴¹ K. Honscheid,⁴² R. Kass,⁴² A. Gaz^{a,43} M. Margoni^{ab,43} M. Posocco^{a,43} G. Simi^{ab,43} F. Simonetto^{ab,43} R. Stroili^{ab,43} S. Akar,⁴⁴ E. Ben-Haim,⁴⁴ M. Bomben,⁴⁴ G. R. Bonneauaud,⁴⁴ G. Calderini,⁴⁴ J. Chauveau,⁴⁴ G. Marchiori,⁴⁴ J. Ocariz,⁴⁴ M. Biasini^{ab,45} E. Manoni^{a,45} A. Rossi^{a,45} G. Batignani^{ab,46} S. Bettarini^{ab,46} M. Carpinelli^{ab,46,††} G. Casarosa^{ab,46} M. Chrzaszcza^{a,46} F. Forti^{ab,46} M. A. Giorgi^{ab,46} A. Lusiani^{ac,46} B. Oberhof^{ab,46} E. Paolomi^{ab,46} M. Rama^{a,46} G. Rizzo^{ab,46} J. J. Walsh^{a,46} L. Zani^{ab,46} A. J. S. Smith,⁴⁷ F. Anullia^{a,48} R. Faccini^{ab,48} F. Ferrarotto^{a,48} F. Ferroni^{a,48,††} A. Pilloni^{ab,48} G. Piredda^{a,48,*} C. Bünger,⁴⁹ S. Dittrich,⁴⁹ O. Grünberg,⁴⁹ M. Heß,⁴⁹ T. Leddig,⁴⁹ C. Voß,⁴⁹ R. Waldi,⁴⁹ T. Adye,⁵⁰ F. F. Wilson,⁵⁰ S. Emery,⁵¹ G. Vasseur,⁵¹ D. Aston,⁵² C. Cartaro,⁵² M. R. Convery,⁵² J. Dorfan,⁵² W. Dunwoodie,⁵² M. Ebert,⁵² R. C. Field,⁵² B. G. Fulsom,⁵² M. T. Graham,⁵² C. Hast,⁵² W. R. Innes,^{52,*} P. Kim,⁵² D. W. G. S. Leith,^{52,*} S. Luitz,⁵² D. B. MacFarlane,⁵² D. R. Muller,⁵² H. Neal,⁵² B. N. Ratcliff,⁵² A. Roodman,⁵² M. K. Sullivan,⁵² J. Va'vra,⁵² W. J. Wisniewski,⁵² M. V. Purohit,⁵³ J. R. Wilson,⁵³ A. Randle-Conde,⁵⁴ S. J. Sekula,⁵⁴ H. Ahmed,⁵⁵ M. Bellis,⁵⁶ P. R. Burchat,⁵⁶ E. M. T. Puccio,⁵⁶ M. S. Alam,⁵⁷ J. A. Ernst,⁵⁷ R. Gorodeisky,⁵⁸ N. Guttman,⁵⁸ D. R. Peimer,⁵⁸ A. Soffer,⁵⁸ S. M. Spanier,⁵⁹ J. L. Ritchie,⁶⁰ R. F. Schwitters,⁶⁰ J. M. Izen,⁶¹ X. C. Lou,⁶¹ F. Bianchi^{ab,62} F. De Mori^{ab,62} A. Filippi^{a,62} D. Gamba^{ab,62} L. Lanceri,⁶³ L. Vitale,⁶³ F. Martinez-Vidal,⁶⁴ A. Oyanguren,⁶⁴ J. Albert^{b,65} A. Beaulieu^{b,65} F. U. Bernlochner^{b,65} G. J. King^{b,65} R. Kowalewski^{b,65} T. Lueck^{b,65} I. M. Nugent^{b,65} J. M. Roney^{b,65} R. J. Sobie^{ab,65} N. Tasneem^{b,65} T. J. Gershon,⁶⁶ P. F. Harrison,⁶⁶ T. E. Latham,⁶⁶ R. Prepost,⁶⁷ and S. L. Wu⁶⁷

(The BABAR Collaboration)

¹Laboratoire d'Annecy-le-Vieux de Physique des Particules (LAPP), Université de Savoie, CNRS/IN2P3, F-74941 Annecy-Le-Vieux, France

²Universitat de Barcelona, Facultat de Fisica, Departament ECM, E-08028 Barcelona, Spain

³INFN Sezione di Bari, I-70126 Bari, Italy

⁴University of Bergen, Institute of Physics, N-5007 Bergen, Norway

⁵Lawrence Berkeley National Laboratory and University of California, Berkeley, California 94720, USA

⁶Ruhr Universität Bochum, Institut für Experimentalphysik 1, D-44780 Bochum, Germany

⁷Institute of Particle Physics^a; University of British Columbia^b, Vancouver, British Columbia, Canada V6T 1Z1

⁸Budker Institute of Nuclear Physics SB RAS, Novosibirsk 630090^a,

Novosibirsk State University, Novosibirsk 630090^b,

Novosibirsk State Technical University, Novosibirsk 630092^c, Russia

⁹University of California at Irvine, Irvine, California 92697, USA

¹⁰University of California at Riverside, Riverside, California 92521, USA

¹¹University of California at Santa Cruz, Institute for Particle Physics, Santa Cruz, California 95064, USA

- ¹²California Institute of Technology, Pasadena, California 91125, USA
¹³University of Cincinnati, Cincinnati, Ohio 45221, USA
¹⁴University of Colorado, Boulder, Colorado 80309, USA
¹⁵Laboratoire Leprince-Ringuet, Ecole Polytechnique, CNRS/IN2P3, F-91128 Palaiseau, France
¹⁶INFN Sezione di Ferrara^a; Dipartimento di Fisica e Scienze della Terra, Università di Ferrara^b, I-44122 Ferrara, Italy
¹⁷INFN Laboratori Nazionali di Frascati, I-00044 Frascati, Italy
¹⁸INFN Sezione di Genova, I-16146 Genova, Italy
¹⁹Harvey Mudd College, Claremont, California 91711, USA
²⁰Humboldt-Universität zu Berlin, Institut für Physik, D-12489 Berlin, Germany
²¹Indian Institute of Technology Guwahati, Guwahati, Assam, 781 039, India
²²University of Iowa, Iowa City, Iowa 52242, USA
²³Iowa State University, Ames, Iowa 50011, USA
²⁴Johns Hopkins University, Baltimore, Maryland 21218, USA
²⁵Université Paris-Saclay, CNRS/IN2P3, IJCLab, F-91405 Orsay, France
²⁶Lawrence Livermore National Laboratory, Livermore, California 94550, USA
²⁷University of Liverpool, Liverpool L69 7ZE, United Kingdom
²⁸Queen Mary, University of London, London, E1 4NS, United Kingdom
²⁹University of London, Royal Holloway and Bedford New College, Egham, Surrey TW20 0EX, United Kingdom
³⁰University of Louisville, Louisville, Kentucky 40292, USA
³¹Johannes Gutenberg-Universität Mainz, Institut für Kernphysik, D-55099 Mainz, Germany
³²University of Manchester, Manchester M13 9PL, United Kingdom
³³University of Maryland, College Park, Maryland 20742, USA
³⁴Massachusetts Institute of Technology, Laboratory for Nuclear Science, Cambridge, Massachusetts 02139, USA
³⁵Institute of Particle Physics^a; McGill University^b, Montréal, Québec, Canada H3A 2T8
³⁶INFN Sezione di Milano^a; Dipartimento di Fisica, Università di Milano^b, I-20133 Milano, Italy
³⁷University of Mississippi, University, Mississippi 38677, USA
³⁸Université de Montréal, Physique des Particules, Montréal, Québec, Canada H3C 3J7
³⁹INFN Sezione di Napoli and Dipartimento di Scienze Fisiche,
Università di Napoli Federico II, I-80126 Napoli, Italy
⁴⁰NIKHEF, National Institute for Nuclear Physics and High Energy Physics, NL-1009 DB Amsterdam, The Netherlands
⁴¹University of Notre Dame, Notre Dame, Indiana 46556, USA
⁴²Ohio State University, Columbus, Ohio 43210, USA
⁴³INFN Sezione di Padova^a; Dipartimento di Fisica, Università di Padova^b, I-35131 Padova, Italy
⁴⁴Laboratoire de Physique Nucléaire et de Hautes Energies, Sorbonne Université,
Paris Diderot Sorbonne Paris Cité, CNRS/IN2P3, F-75252 Paris, France
⁴⁵INFN Sezione di Perugia^a; Dipartimento di Fisica, Università di Perugia^b, I-06123 Perugia, Italy
⁴⁶INFN Sezione di Pisa^a; Dipartimento di Fisica,
Università di Pisa^b; Scuola Normale Superiore di Pisa^c, I-56127 Pisa, Italy
⁴⁷Princeton University, Princeton, New Jersey 08544, USA
⁴⁸INFN Sezione di Roma^a; Dipartimento di Fisica,
Università di Roma La Sapienza^b, I-00185 Roma, Italy
⁴⁹Universität Rostock, D-18051 Rostock, Germany
⁵⁰Rutherford Appleton Laboratory, Chilton, Didcot, Oxon, OX11 0QX, United Kingdom
⁵¹IRFU, CEA, Université Paris-Saclay, F-91191 Gif-sur-Yvette, France
⁵²SLAC National Accelerator Laboratory, Stanford, California 94309 USA
⁵³University of South Carolina, Columbia, South Carolina 29208, USA
⁵⁴Southern Methodist University, Dallas, Texas 75275, USA
⁵⁵St. Francis Xavier University, Antigonish, Nova Scotia, Canada B2G 2W5
⁵⁶Stanford University, Stanford, California 94305, USA
⁵⁷State University of New York, Albany, New York 12222, USA
⁵⁸Tel Aviv University, School of Physics and Astronomy, Tel Aviv, 69978, Israel
⁵⁹University of Tennessee, Knoxville, Tennessee 37996, USA
⁶⁰University of Texas at Austin, Austin, Texas 78712, USA
⁶¹University of Texas at Dallas, Richardson, Texas 75083, USA
⁶²INFN Sezione di Torino^a; Dipartimento di Fisica, Università di Torino^b, I-10125 Torino, Italy
⁶³INFN Sezione di Trieste and Dipartimento di Fisica, Università di Trieste, I-34127 Trieste, Italy
⁶⁴IFIC, Universitat de Valencia-CSIC, E-46071 Valencia, Spain
⁶⁵Institute of Particle Physics^a; University of Victoria^b, Victoria, British Columbia, Canada V8W 3P6
⁶⁶Department of Physics, University of Warwick, Coventry CV4 7AL, United Kingdom
⁶⁷University of Wisconsin, Madison, Wisconsin 53706, USA

Collider searches for dark sectors, new particles interacting only feebly with ordinary matter, have largely focused on identifying signatures of new mediators, leaving much of dark sector structures unexplored. In particular, the existence of dark matter bound states (darkonia) remains to be

investigated. This possibility could arise in a simple model in which a dark photon (A') is light enough to generate an attractive force between dark fermions. We report herein a search for a $J^{PC} = 1^{--}$ darkonium state, the Υ_D , produced in the reaction $e^+e^- \rightarrow \gamma\Upsilon_D, \Upsilon_D \rightarrow A'A'A'$, where the dark photons subsequently decay into pairs of leptons or pions, using 514 fb^{-1} of data collected with the *BABAR* detector. No significant signal is observed, and we set bounds on the $\gamma - A'$ kinetic mixing as a function of the dark sector coupling constant for $0.001 < m_{A'} < 3.16 \text{ GeV}$ and $0.05 < m_{\Upsilon_D} < 9.5 \text{ GeV}$.

PACS numbers: 12.60.-i, 14.80.-j, 95.35.+d

The possibility of dark sectors, new quantum fields neutral under all standard model (SM) forces, has emerged as an intriguing framework to explain the presence of dark matter in the universe [1, 2]. While these particles don't couple directly to ordinary matter, indirect interactions through low-dimensional operators called “portals” are possible [3]. The physics of these dark sectors could involve an arbitrary number of fields and interactions, including the possibility of self-interacting dark matter. This scenario can be realized in a minimal dark sector model containing a single Dirac fermion (χ) charged under a new U(1) gauge group with a coupling constant g_D [4]. The corresponding force carrier is conventionally referred to as a dark photon (A'), and couples to the SM photon via kinetic mixing with strength ε [5, 6]. A light dark photon would give rise to an attractive force between the χ and $\bar{\chi}$ particles, resulting in the formation of bound states (darkonia) when $1.68m_{A'} < \alpha_D m_\chi$ for $\alpha_D = g_D^2/4\pi$ [4, 7].

The two lowest energy bound states in this model are denoted η_D ($J^{PC} = 0^{-+}$) and Υ_D ($J^{PC} = 1^{--}$), in analogy with similar SM states. The quantum numbers predict the following production and decay mechanisms at e^+e^- colliders: $e^+e^- \rightarrow \eta_D + A', \eta_D \rightarrow A'A'$ and initial-state radiation (ISR) process $e^+e^- \rightarrow \Upsilon_D + \gamma_{\text{ISR}}, \Upsilon_D \rightarrow A'A'A'$. In the regime $m_{A'} < 2m_\chi$, the dark photon decays visibly into a pair of SM fermions with a decay width proportional to the product $m_{A'}\varepsilon^2$. Depending on the value of these parameters, the decays can be prompt or significantly displaced from the e^+e^- interaction point. Current constraints on visible A' decays [8–18] exclude values of $\varepsilon \gtrsim 10^{-3}$ over a wide range of masses from the dielectron threshold up to tens of GeV [19].

We report herein a search for darkonium in the ISR process $e^+e^- \rightarrow \gamma_{\text{ISR}}\Upsilon_D, \Upsilon_D \rightarrow A'A'A'$, where the dark photons subsequently decay into pairs of electrons, muons, or pions. The cross section is determined for prompt A' decays in the region $0.001 \text{ GeV} < m_{A'} < 3.16 \text{ GeV}$ and $0.05 \text{ GeV} < m_{\Upsilon_D} < 9.5 \text{ GeV}$. For $m_{A'} < 0.2 \text{ GeV}$, the dark photon decay length becomes significant for values of ε we expect to probe, and we additionally report cross sections for lifetimes $\tau_{A'}$ corresponding to $c\tau_{A'}$ values of 0.1, 1, and 10 mm. This search is based on 514 fb^{-1} of data collected with the *BABAR* detector at the SLAC PEP-II e^+e^- collider at the $\Upsilon(4S)$, $\Upsilon(3S)$, and $\Upsilon(2S)$ resonances and their vicinities [20]. The *BABAR* de-

tector is described in detail elsewhere [21, 22]. To avoid experimental bias, the data are not examined until the selection procedure is finalized. The analysis is developed using simulated signal events and a small fraction of real data for background studies.

Signal events are generated using MadGraph5 [23] with prompt dark photon decays for 119 different A' and Υ_D mass hypotheses. For $m_{A'} < 0.2 \text{ GeV}$, we also simulate samples with non-zero dark photon lifetimes corresponding to proper decay lengths 0.1 mm, 1 mm, and 10 mm. The detector acceptance and reconstruction efficiencies are estimated with a simulation based on GEANT4 [24]. Since the background is too complex to be accurately simulated, we use 5% of the data to optimize the selection criteria, assuming that any signal component has a negligible impact on this procedure. This data set, referred to as the optimization sample, is discarded from the final results.

The event selection for prompt A' decays proceeds by selecting events containing exactly six charged tracks, and reconstructing dark photon candidates as pairs of oppositely charged tracks identified as electrons, muons, or pions by particle identification algorithms. We require the presence of at least one lepton pair of opposite charge with the same flavor to limit the large accidental background. We form Υ_D candidates by combining three dark photon candidates, and fit them, constraining all tracks to originate from a common point compatible with the beam interaction region. For each Υ_D candidate, we additionally form same-sign track combinations by swapping particles with identical flavor between reconstructed A' pairs, such as $(e^+e^+)(e^-e^-)(\mu^+\mu^-)$ or $(\pi^+\pi^+)(\pi^-\pi^-)(e^+e^-)$. For the fully mixed final state $(\mu^+\mu^-)(\pi^+\pi^-)(e^+e^-)$, we use the same-sign combination $(\mu^+\pi^+)(\mu^-\pi^-)(e^+e^-)$, since pions are more easily misidentified as muons than electrons. The mass difference between same-sign pairs, distributed more broadly for signal events than for combinatorial background, is used to further improve the signal selection as discussed below.

The detection of the ISR photon accompanying Υ_D production is not explicitly required. Instead, we infer the kinematics of the particle recoiling against the Υ_D candidates, and we select the ISR photon candidate that is most compatible with the photon hypothesis as follows. If the recoil particle is determined to have been emit-

ted inside the electromagnetic calorimeter acceptance, we search for the presence of a corresponding ISR photon candidate, which is defined as a neutral cluster having an energy within 10% of that of the recoiling particle, and an angle compatible with the direction of the recoiling particle to better than 0.1 rad.

To improve the signal purity, we train three multivariate classifiers consisting of logistic regressions stacked on top of Random Forest (RF) classifiers [25]. The following 13 variables are used as inputs to the RF: the χ^2 of the constrained fit to the Υ_D candidate; combined particle identification information of the six tracks; the maximum mass difference between any pair of A' candidates; the polar angle and the invariant mass of the particle recoiling against the reconstructed Υ_D candidate; a categorical feature indicating whether the recoiling particle is emitted inside the calorimeter acceptance and if a corresponding ISR photon candidate is found; the sum of neutral energy deposited in the electromagnetic calorimeter, excluding the ISR photon candidate; the average of the three dark photon helicity angles [26]; the average of the angles between pairs of dark photons in the Υ_D rest frame; the average of the dihedral angles between pairs of dark photons; the average of the three helicity angles of the tracks produced in the A' decays; the average of the dark photon decay lengths, defined as the distances between the primary interaction point and the A' decay vertices; and the maximum mass difference between same-sign pairs.

To improve the robustness of the predictions of the classifiers, we group the final states into three categories based on the number of pion pairs: zero (C_0), one (C_1), or two (C_2) pion pairs. A classifier is trained for each category with a sample of simulated events for different Υ_D and A' masses and a fraction of the optimization sample to describe the background. The classifier outputs are then transformed into classifier scores using a logit function [27], with higher scores indicating greater probabilities of being signal events. The distribution of the classifier scores for each category are shown in Fig. 1. The optimal selection criteria are determined by maximizing a figure of merit averaged over a wide range of Υ_D and A' masses. We adopt a conservative approach and treat observed events as signal candidates for the purposes of calculating the figure of merit. If multiple Υ_D candidates are selected in an event, a single one is chosen based on its final state according to the following sequence of hypotheses: 6e, 4e2 μ , 2e4 μ , 6 μ , 4e2 π , 2e2 μ 2 π , 4 μ 2 π , 2e4 π , 2 μ 4 π .

A total of 69 events pass all the selection criteria. The corresponding $(m_{\Upsilon_D}, m_{A'})$ distribution is shown in Fig. 2. The events near $m_{\Upsilon_D} \sim 0.1$ GeV and $m_{A'} \sim 0.05$ GeV arise from $e^+e^- \rightarrow \gamma\gamma\gamma$ events in which all three photons convert to e^+e^- pairs.

The signal is extracted by combining all event categories into a single sample, and scanning the $(m_{\Upsilon_D}, m_{A'})$

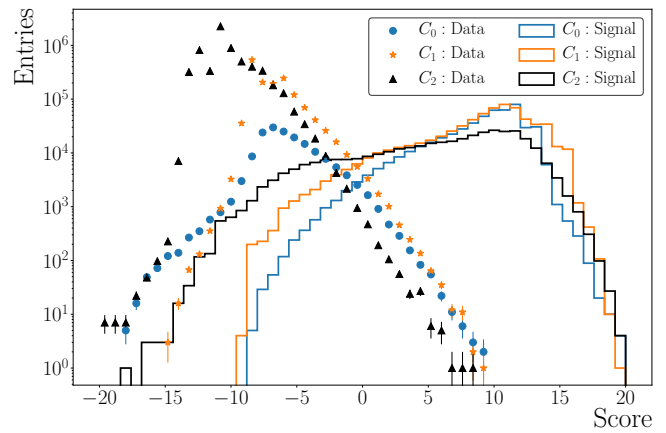


FIG. 1: The distribution of the classifier scores for each event category for the data (markers) and signal Monte Carlo (solid lines) samples. The MC simulations are arbitrarily normalized.

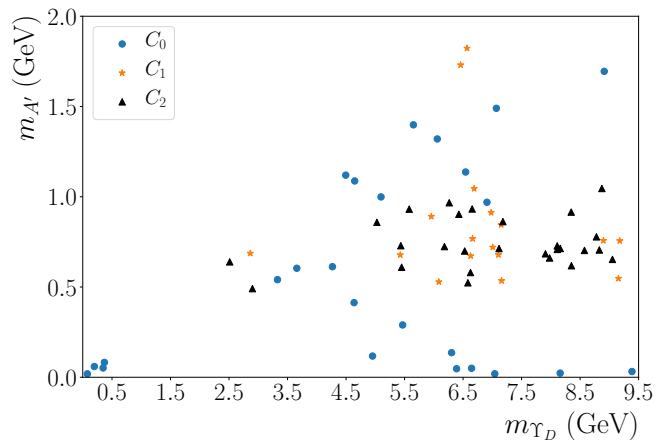


FIG. 2: The $(m_{\Upsilon_D}, m_{A'})$ distribution for events passing all selection criteria for prompt dark photon decays.

plane in steps of the signal resolution. The signal region for a given mass hypothesis is defined as the interval $[m_{\Upsilon_D} - 4\sigma_{m_{\Upsilon_D}}; m_{\Upsilon_D} + 4\sigma_{m_{\Upsilon_D}}]$ and $[m_{A'} - 4\sigma_{m_{A'}}; m_{A'} + 4\sigma_{m_{A'}}]$, where $\sigma_{m_{\Upsilon_D}}$ ($\sigma_{m_{A'}}$) denotes the corresponding Υ_D (A') mass resolution. The resolutions are determined by fitting the different signal Monte Carlo (MC) samples with a Crystal Ball function [28] and interpolating the results throughout the full mass range. The Υ_D (A') mass resolution varies between 5 – 40 MeV (1 – 8 MeV); the detailed results are available in the Supplemental Material [29]. The number of observed background events is estimated by averaging two neighboring regions along the m_{Υ_D} axis: $[m_{\Upsilon_D} - 8\sigma_{m_{\Upsilon_D}}; m_{\Upsilon_D} - 4\sigma_{m_{\Upsilon_D}}]$ and $[m_{\Upsilon_D} + 4\sigma_{m_{\Upsilon_D}}; m_{\Upsilon_D} + 8\sigma_{m_{\Upsilon_D}}]$. This choice is motivated by the potential background contribution due to hadronic resonances or photon conversions, which would be concentrated at similar values of dark photon masses. The signal significance is assessed from MC samples, using

sideband data from the classifier score distribution to model the $(m_{\Upsilon_D}, m_{A'})$ distribution of the background. The most significant measurement contains two events in the signal window, corresponding to a p-value of 30%, which is compatible with the null hypothesis.

In the absence of signal, we derive 90% confidence level (CL) upper limits on the $e^+e^- \rightarrow \gamma\Upsilon_D$ cross section using a profile likelihood method [30]. The probability of observing N events in a given signal region is described by the following model:

$$P(N|n+b) = \frac{e^{-n} n^N}{N!} \frac{e^{-b} b^B}{B!} \frac{1}{2\pi\sigma_Z\sigma_L} e^{-\frac{(z-z)^2}{2\sigma_Z^2}} e^{-\frac{(l-L)^2}{2\sigma_L^2}}$$

where b (B) is the expected (estimated) number of background events, and $n = l z \sigma(e^+e^- \rightarrow \gamma\Upsilon_D)$ is the expected number of signal events given by the product of the integrated luminosity l , the $e^+e^- \rightarrow \gamma\Upsilon_D$ cross section, and the signal efficiency z . The measured luminosity, signal efficiency, and their uncertainties are denoted by L , Z , σ_L , and σ_Z , respectively. The signal efficiency includes the dark photon branching fractions, taken from Ref. [31]. The efficiency is determined for each simulated sample and interpolated to the full parameter space, ranging from 0.1% for $m_{\Upsilon_D} \sim 0.15$ GeV, $m_{A'} \sim 0.05$ GeV to 34% for $m_{\Upsilon_D} \sim 8.0$ GeV, $m_{A'} \sim 1.0$ GeV. The uncertainty in the signal efficiency arises mainly from particle identification algorithms, assessed with high-purity samples of leptons and pions. This source of uncertainty varies between 9% and 11%. The uncertainty associated with the efficiency extrapolation procedure ranges from 4% to 7%, depending on the m_{Υ_D} and $m_{A'}$. Other uncertainties include the tracking efficiency (1.2%) and the limited statistical precision of the simulated sample (1%-5%). The uncertainty in the dark photon branching fraction [31] ranges from parts per mille to 1%. The uncertainty in the luminosity is determined to be 0.6% [20]. The cross section at 90% CL upper limits are displayed in Fig. 3. The dark photon decays predominantly into $\pi^+\pi^-\pi^0$ (K^+K^-) near the ω (ϕ) resonance which are not considered in this analysis, resulting in much looser bounds around $m_{A'} \sim 0.8$ GeV ($m_{A'} \sim 1$ GeV).

We follow a similar procedure to determine the $e^+e^- \rightarrow \gamma\Upsilon_D$ cross section for each dark photon lifetime hypothesis. The measurement is performed for $m_{A'} < 0.2$ GeV. In this mass range, the A' decays almost exclusively to an e^+e^- pair. The event selection is analogous to that previously described, except that we constrain the momentum vector of the A' candidates to point back to the beam interaction region instead of requiring the tracks to originate from this location when performing the Υ_D kinematic fit. To further suppress photon conversions in the detector material, we add the following variables to the RF classifier, averaged over the three dark photon candidates: the χ^2 of a fit of the A' candidate; the angle between the secondary vertex flight direction and the A' momentum; and the ratio between

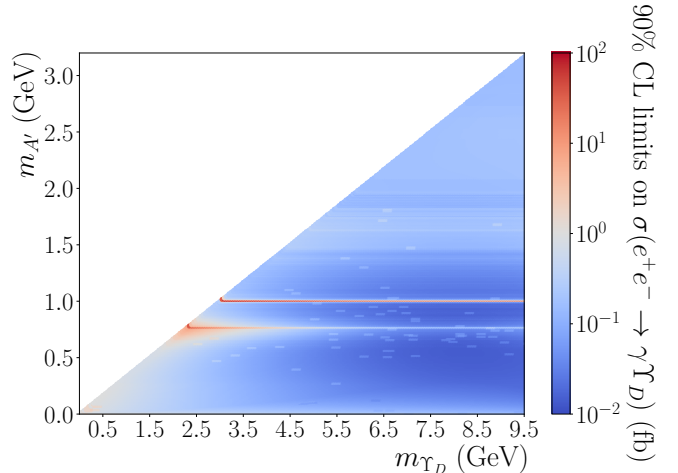


FIG. 3: The 90% CL upper limits on the $e^+e^- \rightarrow \gamma\Upsilon_D$ cross section for prompt dark photon decays.

the flight length and its uncertainty. We train a classifier for each $c\tau_{A'}$ value to improve the search sensitivity. A total of 56, 33, and 31 events are selected for the $c\tau_{A'} = 0.1$, 1, and 10 mm data sample, respectively. The resulting mass distributions are shown in Fig. 4. The signal extraction procedure described above is applied to each selected sample separately. No significant signal is observed for any A' lifetime hypothesis, and limits on the cross section for each value of $c\tau_{A'}$ are extracted. The classifier score distributions and the cross section at 90% CL upper limits are shown in the Supplemental Material [29].

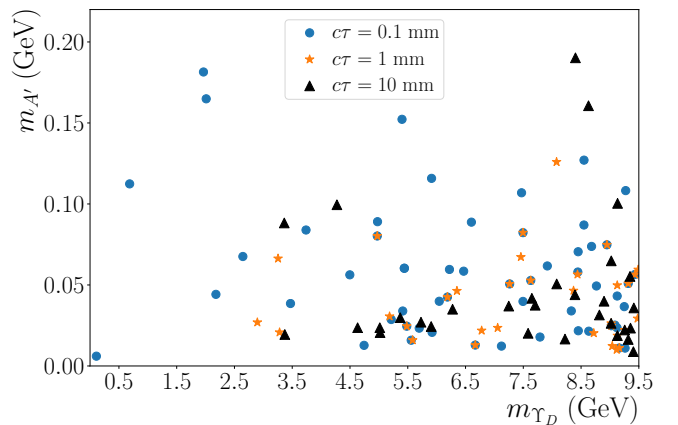


FIG. 4: The $(m_{\Upsilon_D}, m_{A'})$ mass distribution of event candidates passing all selection criteria for the datasets optimized for each dark photon lifetime.

The 90% CL upper limits on the kinetic mixing parameter are extracted by an iterative procedure taking into account the effect of the potentially long dark photon lifetime. At each step, we estimate the dark photon lifetime given the current value of the kinetic mixing, compare

the limit on the production cross section interpolated at that lifetime, update the kinetic mixing, and repeat the procedure until convergence is obtained. Since the dark photon lifetime is independent of the dark sector coupling constant, we derive separate limits for α_D values set to 0.1, 0.3, 0.5, 0.7, 0.9, and 1.1. The results are shown in Fig. 5 for $\alpha_D = 0.5$, and in the Supplemental Material [29] for the remaining values. Bounds on the mixing strength ε down to $5 \times 10^{-5} - 10^{-3}$ are set for a large fraction of the parameter space. Constraints for different values of α_D , $m_{A'}$ and m_{Υ_D} are also shown in Fig. 6.

In summary, we report the first search for a dark sector bound state decaying into three dark photons in the range $0.001 \text{ GeV} < m_{A'} < 3.16 \text{ GeV}$ and $0.05 \text{ GeV} < m_{\Upsilon_D} < 9.5 \text{ GeV}$. No significant signal is seen, and we derive limits on the $\gamma - A'$ kinetic mixing ε at the level of $5 \times 10^{-5} - 10^{-3}$, depending on the values of the model parameters. These measurements improve upon existing constraints over a significant fraction of dark photon masses below 1 GeV for large values of the dark sector coupling constant.

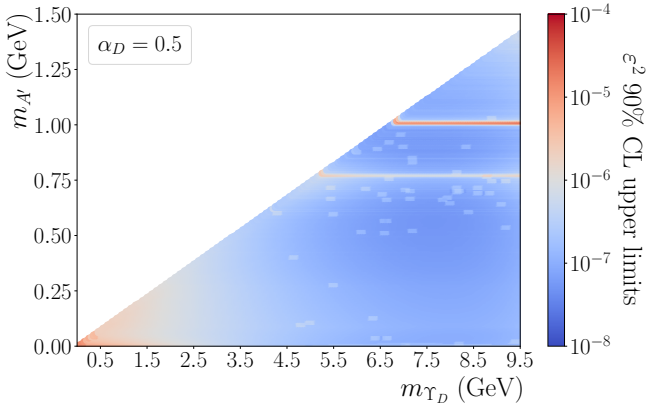


FIG. 5: The 90% CL upper limits on the kinetic mixing ε as a function of the Υ_D mass, m_{Υ_D} , and dark photon mass, $m_{A'}$, assuming $\alpha_D = 0.5$.

The authors wish to thank Haipeng An and Yue Zhang for useful discussions and for providing us with MadGraph simulations of self-interacting dark matter processes. We also thank Gaia Lanfranchi for providing us constraints from existing experiments. We are grateful for the extraordinary contributions of our PEP-II colleagues in achieving the excellent luminosity and machine conditions that have made this work possible. The success of this project also relies critically on the expertise and dedication of the computing organizations that support *BABAR*. The collaborating institutions wish to thank SLAC for its support and the kind hospitality extended to them. This work is supported by the US Department of Energy and National Science Foundation, the Natural Sciences and Engineering Research Council (Canada), the Commissariat à l’Energie Atom-

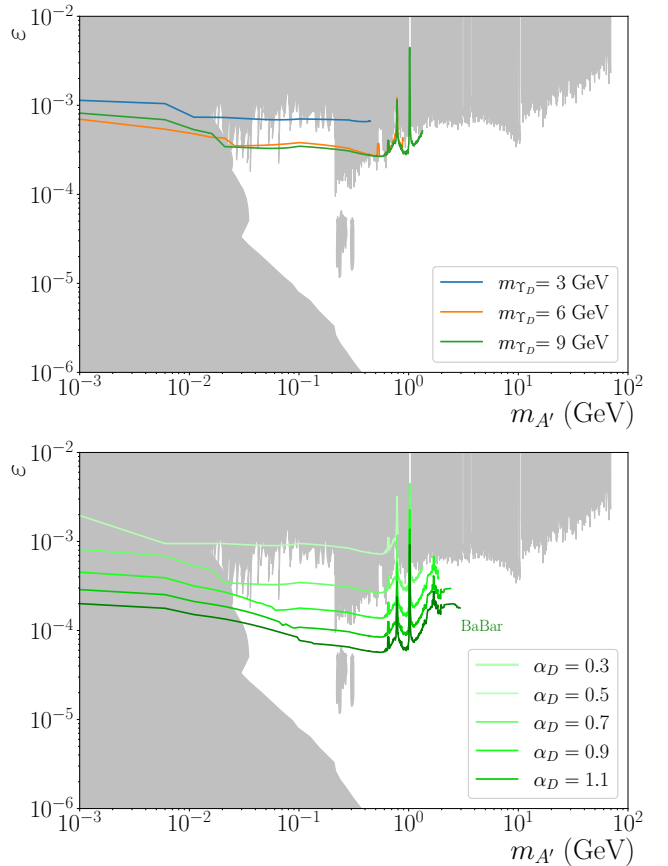


FIG. 6: The 90% CL upper limits on the kinetic mixing ε for (top) various Υ_D masses assuming $\alpha_D = 0.5$ and (bottom) various α_D values assuming $m_{\Upsilon_D} = 9 \text{ GeV}$ together with current constraints (gray area) [8–18].

ique and Institut National de Physique Nucléaire et de Physique des Particules (France), the Bundesministerium für Bildung und Forschung and Deutsche Forschungsgemeinschaft (Germany), the Istituto Nazionale di Fisica Nucleare (Italy), the Foundation for Fundamental Research on Matter (The Netherlands), the Research Council of Norway, the Ministry of Education and Science of the Russian Federation, Ministerio de Economía y Competitividad (Spain), the Science and Technology Facilities Council (United Kingdom), and the Binational Science Foundation (U.S.-Israel). Individuals have received support from the Marie-Curie IEF program (European Union) and the A. P. Sloan Foundation (USA).

* Deceased

[†] Now at: Wuhan University, Wuhan 430072, China

[‡] Now at: Università di Bologna and INFN Sezione di Bologna, I-47921 Rimini, Italy

[§] Now at: King’s College, London, WC2R 2LS, UK

[¶] Now at: University of Huddersfield, Huddersfield HD1

3DH, UK

** Now at: University of South Alabama, Mobile, Alabama 36688, USA

†† Also at: Università di Sassari, I-07100 Sassari, Italy

‡‡ Also at: Gran Sasso Science Institute, I-67100 L'Aquila, Italy

- [1] M. Pospelov, A. Ritz, and M. B. Voloshin, Phys. Lett. B **662**, 53 (2008).
- [2] N. Arkani-Hamed, D. P. Finkbeiner, T. R. Slatyer, and N. Weiner, Phys. Rev. D **79**, 015014 (2009).
- [3] J. Beacham, C. Burrage, D. Curtin, A. De Roeck, J. Evans, J. L. Feng, C. Gatto, S. Gninenko, A. Hartin and I. Irastorza *et al.*, J. Phys. G **47**, 010501 (2020).
- [4] H. An, B. Echenard, M. Pospelov, and Y. Zhang, Phys. Rev. Lett. **116**, 151801 (2016).
- [5] P. Fayet, Nucl. Phys. B **187**, 184 (1981).
- [6] B. Holdom, Phys. Lett. B **166**, 196 (1986).
- [7] F. J. Rogers, H. C. Grabske Jr., and D. J. Harwood, Phys. Rev. A **1**, 1577 (1970).
- [8] E. M. Riordan, M. W. Krasny, K. Lang, P. De Barbaro, A. Bodek, S. Dasu, N. Varelas, X. Wang, R. G. Arnold, and D. Benton *et al.* Phys. Rev. Lett. **59**, 755 (1987).
- [9] J. D. Bjorken, S. Ecklund, W. R. Nelson, A. Abashian, C. Church, B. Lu, L. W. Mo, T. A. Nunamaker, and P. Rassmann, Phys. Rev. D **38**, 3375 (1988).
- [10] A. Bross, M. Crisler, S. H. Pordes, J. Volk, S. Errede, and J. Wrbanek, Phys. Rev. Lett. **67**, 2942 (1991).
- [11] M. Davier and H. Nguyen Ngoc, Phys. Lett. B **229**, 150 (1989).
- [12] J. Blümlein and J. Brunner, Phys. Lett. B **731**, 320 (2014).
- [13] D. Curtin, R. Essig, S. Gori, P. Jaiswal, A. Katz, T. Liu, Z. Liu, D. McKeen, J. Shelton, and M. Strassler *et al.* Phys. Rev. D **90**, 075004 (2014).
- [14] J. P. Lees *et al.* [BABAR Collaboration], Phys. Rev. Lett. **113**, 201801 (2014).
- [15] J. R. Batley *et al.* [NA48/2 Collaboration], Phys. Lett. B **746**, 178 (2015).
- [16] A. Anastasi *et al.* [KLOE-2 Collaboration], Phys. Lett. B **757**, 356 (2016).
- [17] D. Banerjee *et al.* [NA64 Collaboration], Phys. Rev. Lett. **120**, 231802 (2018).
- [18] R. Aaij *et al.* [LHCb Collaboration], Phys. Rev. Lett. **124**, 041801 (2020).
- [19] Natural units ($\hbar = c = 1$) are used throughout this paper.
- [20] J. P. Lees *et al.* [BABAR Collaboration], Nucl. Instrum. Meth. A **726**, 203 (2013).
- [21] B. Aubert *et al.* [BABAR Collaboration], Nucl. Instrum. Meth. A **479**, 1 (2002).
- [22] B. Aubert *et al.* [BABAR Collaboration], Nucl. Instrum. Meth. A **729**, 615 (2013).
- [23] J. Alwall, R. Frederix, S. Frixione, V. Hirschi, F. Maltoni, O. Mattelaer, H. S. Shao, T. Stelzer, P. Torrielli, and M. Zaro, JHEP **07**, 079 (2014).
- [24] S. Agostinelli *et al.* [GEANT4 Collaboration], Nucl. Instrum. Meth. A **506**, 250 (2003).
- [25] L. Breiman, Machine Learning **45**, 5 (2001).
- [26] The helicity angle is defined as the angle between the γ_D momentum in the center-of-mass frame and the dark photon momentum in the γ_D rest frame.
- [27] J. Berkson, Journal of the American Statistical Association **39** 227 (1944).
- [28] M. J. Oreglia, Ph.D Thesis, SLAC, 4158 (1981).
- [29] See Supplemental Material at <http://XXX> for additional

plots.

- [30] W. A. Rolke, A. M. Lopez, and J. Conrad, Nucl. Instrum. Meth. A **551**, 493 (2005).
- [31] B. Batell, M. Pospelov, and A. Ritz, Phys. Rev. D **79**, 115008 (2009).

Supplemental Material for *BABAR-PUB-21/002*

Search for Darkonium in e^+e^- Collisions

Additional figures for the dark sector bound state search are presented in this Supplemental Material.

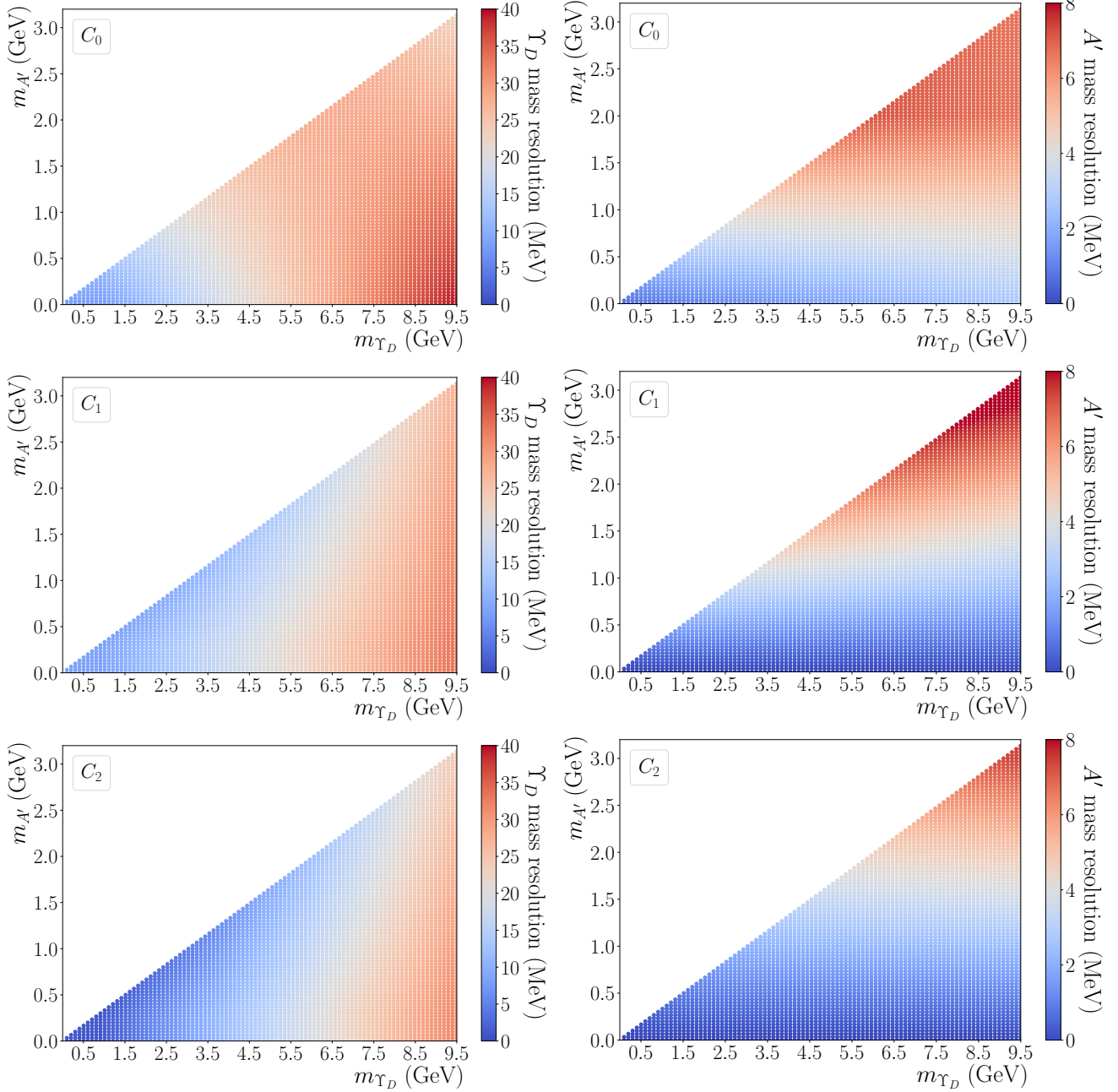


FIG. 7: The Υ_D and A' mass resolution for each category of events (see text) for prompt A' decays.

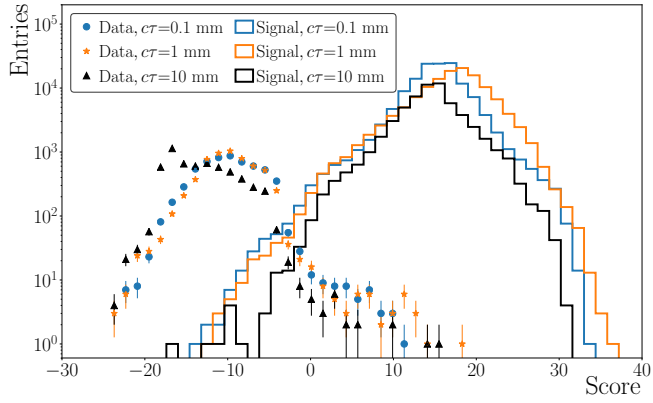


FIG. 8: The distribution of the classifier scores for data (markers) and signal MC simulations (solid lines) for dark photon lifetimes corresponding to (top) $c\tau_{A'} = 0.1$ mm, (middle) $c\tau_{A'} = 1$ mm, and (bottom) $c\tau_{A'} = 10$ mm. The MC simulations are arbitrarily normalized.

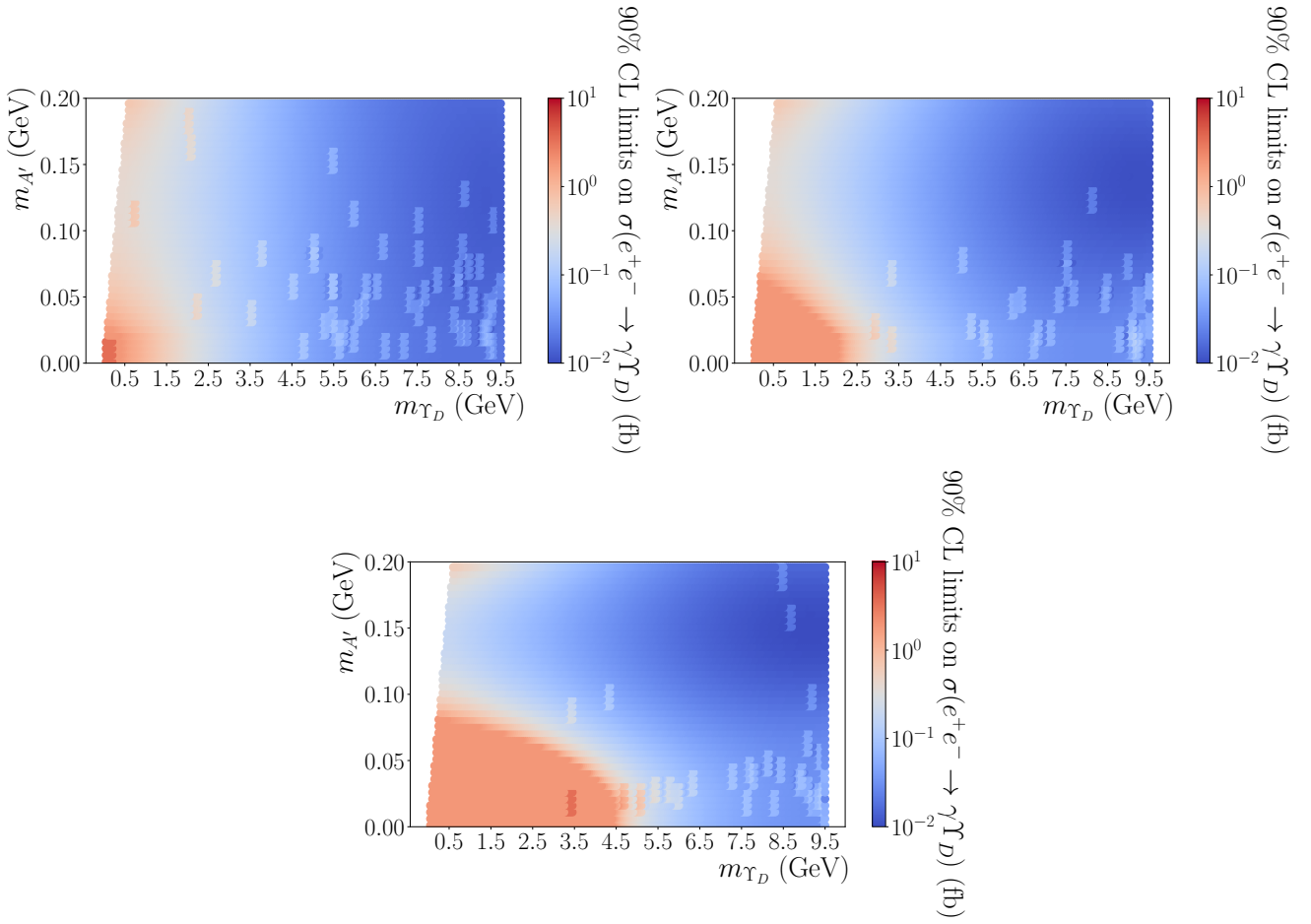


FIG. 9: The 90% CL upper limits on the $e^+e^- \rightarrow \gamma\Gamma_D$ cross section for dark photon lifetimes corresponding to (top left) $c\tau_{A'} = 0.1$ mm, (top right) $c\tau_{A'} = 1$ mm, and (bottom) $c\tau_{A'} = 10$ mm.

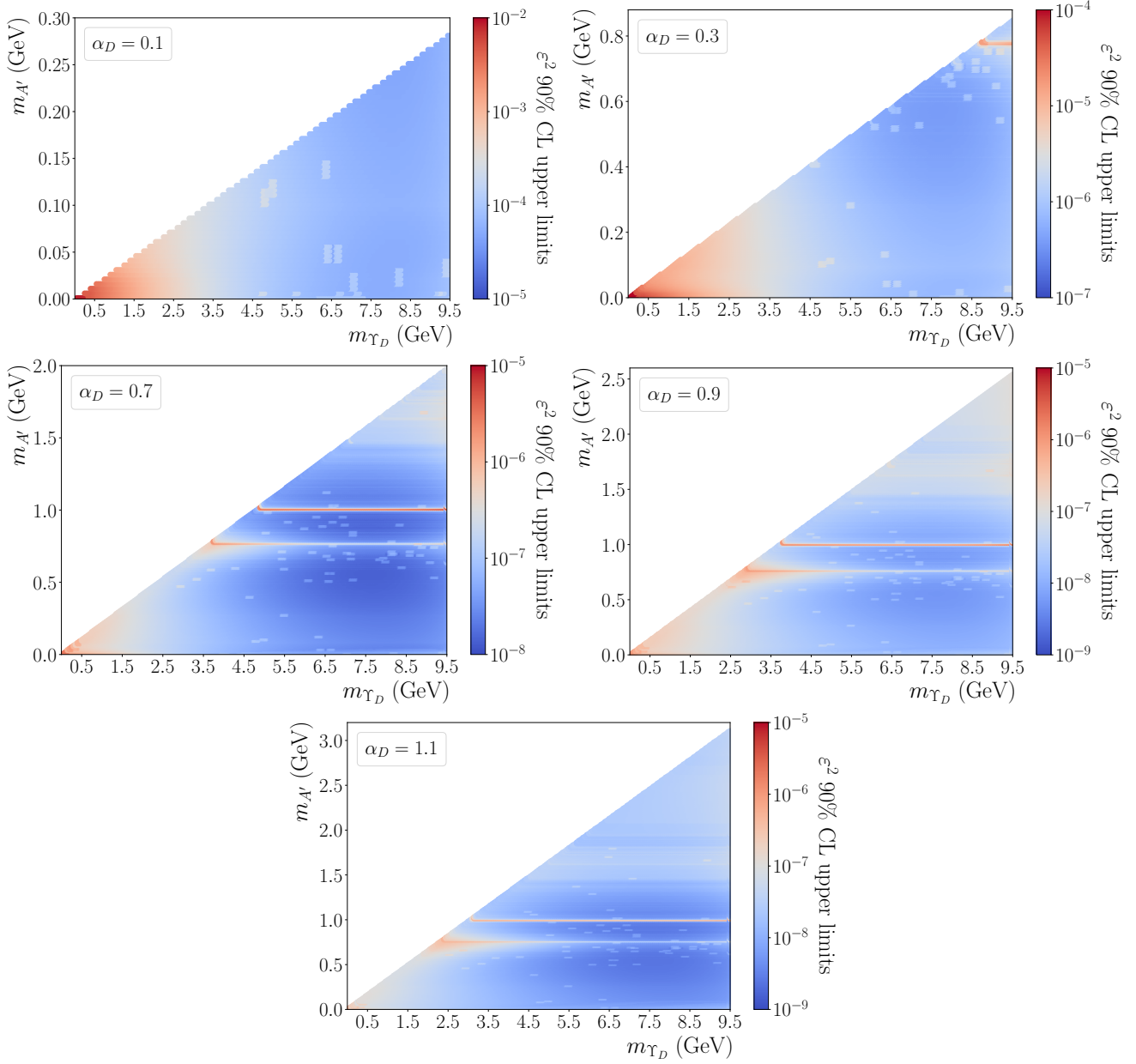


FIG. 10: The 90% CL upper limits on the kinetic mixing ε^2 as a function of the γ_D mass, m_{γ_D} , and dark photon mass, $m_{A'}$, assuming (top left) $\alpha_D = 0.1$, (top right) $\alpha_D = 0.3$, (middle left) $\alpha_D = 0.7$, (middle right) $\alpha_D = 0.9$, and (bottom) $\alpha_D = 1.1$.